

ANALYSIS OF TRANSIENT ELECTROMAGNETIC SCATTERING USING THE MULTILEVEL TIME DOMAIN FAST DIPOLE METHOD

J. Ding^{*}, L. Yu, W. Xu, C. Gu, and Z. Li

College of Electronic and Information Engineering, Nanjing University of Aeronautics and Astronautics, Nanjing 210016, China

Abstract—In this paper, a multilevel time domain fast dipole method (TD-FDM) is proposed for solving time-domain magnetic field integral equations. It is the extension of TD-FDM to the multilevel. This proposed scheme starts by multilevel grouping. At each level, the far-field interaction can be expanded through the Taylor series and reconstructed via aggregation-translation-disaggregation procedure, which reduces the memory requirement and the computational cost of the marching-on in-time (MOT) method. Numerical results about the electromagnetic scattering from perfect electric conductor (PEC) objects are given to demonstrate the validity and efficiency of the proposed scheme.

1. INTRODUCTION

Marching-on-in-time (MOT) schemes for solving time-domain integral-equation (TDIE) [1–6] methods have been widely used to analyze electromagnetic scattering from perfectly electric conducting (PEC) objects. Compared with FDTD [7, 8], it only requires a discretization of the scatterer surface. Unfortunately, the MOT scheme suffers from tremendously high computational cost and memory requirement as the electrical size of the scatterers increases. In the past decades, many fast algorithms have been presented to reduce the memory requirement and the computational complexity of the MOT method, such as the plane wave time domain (PWTD) algorithm [9, 10], the multilevel PWTD algorithm [11], and time domain adaptive integral equation method (TD-AIM) [12, 13].

More recently, the time domain equivalent dipole moment (TD-EDM) method [14, 15] has been developed to simplify and accelerate

Received 10 April 2013, Accepted 22 May 2013, Scheduled 10 June 2013

* Corresponding author: Ji Ding (dingji@nuaa.edu.cn).

the computation of impedance matrix in the TDIE method. In the TD-EDM method, the surface current distribution containing two adjacent triangles is replaced by an infinitely small dipole with an equivalent dipole moment. The major advantage is that the impedance matrix element can be expressed using simplified form, which avoids the usual double integrals and cuts down the matrix-filling time significantly. However, the TD-EDM method does not change matrix vector product operations and the memory requirement.

In this paper, a multilevel time domain fast dipole method (TD-FDM) is proposed for solving the electromagnetic scattering from PEC targets. The proposed scheme builds upon the authors' previous work TD-FDM reported in [16–19]. It is the extension of the single level TD-FDM [16] to the multilevel. The algorithm starts by grouping in multilevel fashion, the spatial basis functions into geometrically equal-sized groups. At each level, if two groups qualify as far-field pair and their parent groups do not qualify as far-field pair, the transient field can be expanded through the Taylor series and reconstructed via aggregation-translation-disaggregation procedure. Moreover, it can reduce the solution time and the memory requirement.

This paper is organized as follows. Section 2 reviews the TD-EDM method for solving time domain integral equation. Section 3 details the principle and implementation of multilevel TD-FDM scheme. Section 4 gives several numerical results to demonstrate the validity of the proposed method which is followed by our conclusions.

2. REVIEW OF THE TD-EDM METHOD

Consider a closed PEC body with surface S residing in free space, excited by an incident electromagnetic field. This transient field will result a surface current $\mathbf{J}(\mathbf{r}, t)$ on S that generates a scattered field. Enforcing the boundary conditions on the surface of the conductors, the time-domain magnetic field integral equations (MFIE) formulation is obtained

$$\hat{\mathbf{n}} \times [\mathbf{H}^i(\mathbf{r}, t) + \mathbf{H}^s(\mathbf{r}, t)] = \mathbf{J}(\mathbf{r}, t), \quad (1)$$

where $\hat{\mathbf{n}}$ represents the outward normal vector to S . The surface current density $\mathbf{J}(\mathbf{r}, t)$ can be approximately expanded as

$$\mathbf{J}(\mathbf{r}, t) = \sum_{n=1}^{N_s} \mathbf{f}_n(\mathbf{r}) I_n(t) = \sum_{n=1}^{N_s} \mathbf{f}_n(\mathbf{r}) \sum_{j=1}^{N_t} I_{n,j} T_j(t). \quad (2)$$

Here, $\mathbf{f}_n(\mathbf{r})$ is the RWG basis functions, $T_j(t) = T(t - j\Delta t)$ (Δt is the time step size) the temporal basis function, and the $I_{n,j}$ the unknown expansion coefficient.

If the electric size of the RWG basis function is sufficiently small, we can assume that the surface current distribution does not change. Based on this assumption, when the observation point is far away from the RWG element, the fields radiated by the current in an RWG element can be approximated as the fields of an infinitely small dipole with an equivalent moment as shown in Fig. 1. The dipole $\mathbf{m}_n(t)$ can be obtained by the integration of the surface current

$$\mathbf{m}_n(t) = \int_{T_n^\pm} \mathbf{J}_n(\mathbf{r}, t) dS = \mathbf{m}_n \sum_{j=1}^{N_t} I_{n,j} T_j(t) = \mathbf{m}_n I_n(t), \quad (3)$$

where $\mathbf{m}_n = l_n(\mathbf{r}_n^{c-} - \mathbf{r}_n^{c+})$. l_n is the length of the common edge, and $\mathbf{r}_n^{c\pm}$ are the centers of T_n^\pm . Referring to [14] and considering Eq. (3), the radiated magnetic fields of the dipole $\mathbf{m}_n(t)$ can be expressed as

$$\mathbf{H}_n^s(\mathbf{r}, t) = \frac{1}{4\pi} (\mathbf{m}_n \times \mathbf{R}) \left[\frac{1}{cR^2} \partial_t I_n(\tau) + \frac{1}{R^3} I_n(\tau) \right], \quad (4)$$

where $\mathbf{R} = \mathbf{r} - \mathbf{r}'$ and $R = |\mathbf{R}|$. c is the speed of light in free space, and $\tau = t - R/c$ denotes the retarded time.

Substituting Eq. (4) into Eq. (1) and applying a spatial Galerkin testing procedure at $t_i = i\Delta t$ leads to a set of equations that can be represented in matrix form as

$$\mathbf{Z}_0 \mathbf{I}_i = \mathbf{V}_i - \sum_{j=0}^{i-1} \mathbf{Z}_{i-j} \mathbf{I}_j, \quad (5)$$

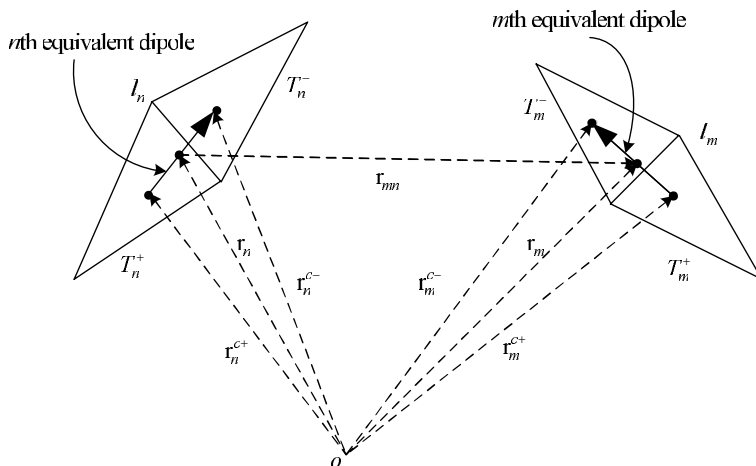


Figure 1. Configuration of the source and the testing functions.

for $0 \leq i \leq N_t$. \mathbf{I}_i is a vector of the weights $I_{n,j}$. The matrix element that satisfy the EDM assumption can be expressed as

$$[\mathbf{Z}_k]_{mn} = \frac{1}{4\pi} (\mathbf{m}_m \times \hat{\mathbf{n}}_m) \cdot (\mathbf{m}_n \times \mathbf{R}) \left[\frac{1}{cR^2} \partial_t T_j(\tau) + \frac{1}{R^3} T_j(\tau) \right] \Big|_{t=k\Delta t}. \quad (6)$$

Note that Eq. (6) does not evaluating the surface integrals, which greatly simplifies the matrix element computation and makes matrix-filling efficient.

3. THE MULTILEVEL TIME DOMAIN FAST DIPOLE METHOD

3.1. Key Idea of the TD-FDM

To alleviate the computational bottleneck of the right-hand side (RHS) in Eq. (5), we introduce the time domain fast dipole method (TD-FDM). The first step of the TD-FDM is to distribute all the basis functions into small equal-sized cubes. Each cube is called a group and the side length of each group is D . If the two cubes are well separated by βD ($\beta \geq 1$), we assume they are a far-field pair. Now let us consider a far-field group pair as shown in Fig. 2. The source group G_i contains the equivalent dipole \mathbf{m}_n located at \mathbf{r}_n and the observation group G_j contains the equivalent dipole \mathbf{m}_m located at \mathbf{r}_m . The centers of the two groups are located at \mathbf{r}_i and \mathbf{r}_j , respectively. The vector \mathbf{R} connecting the two dipoles can be written by

$$\mathbf{R} = \mathbf{r}_{mj} + \mathbf{r}_{ji} - \mathbf{r}_{ni} = \mathbf{R}_m - \mathbf{R}_n, \quad (7)$$

where $\mathbf{r}_{ji} = \mathbf{r}_j - \mathbf{r}_i$, $\mathbf{r}_{mj} = \mathbf{r}_m - \mathbf{r}_j$, $\mathbf{r}_{ni} = \mathbf{r}_n - \mathbf{r}_i$, $\mathbf{R}_m = \mathbf{r}_{mj} + \mathbf{r}_{ji}/2$, and $\mathbf{R}_n = \mathbf{r}_{ni} - \mathbf{r}_{ji}/2$. The time signal $I_n(t)$ can be divided into L consecutive subsignals $I_{n,k}(t)$, each subsignal duration is $T_s = M_t \Delta t$

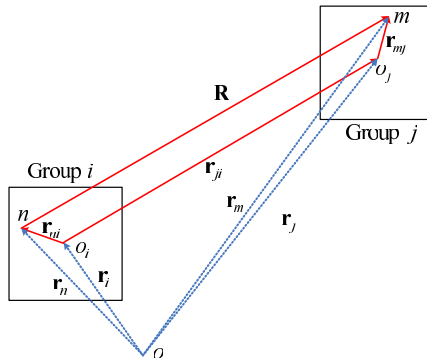


Figure 2. Configuration of a far-field group pair.

($LM_t = N_t$). In keeping with this division, the dipole $\mathbf{m}_n(t)$ can be expressed as

$$\mathbf{m}_n(t) = \mathbf{m}_n I_n(t) = \mathbf{m}_n \sum_{k=1}^L I_{n,k}(t), \tag{8}$$

where

$$I_{n,k}(t) = \sum_{j=(k-1)M_t+1}^{kM_t} I_{n,j} T_j(t). \tag{9}$$

Then, the magnetic field $\mathbf{H}_{n,k}^s(\mathbf{r}, t)$ in the observation associated with the k -th time subsignal can be written as

$$\mathbf{H}_{n,k}^s(\mathbf{r}, t) = \frac{1}{4\pi} (\mathbf{m}_n \times \mathbf{R}) \left[\frac{1}{cR^2} \partial_t I_{n,k}(\tau) + \frac{1}{R^3} I_{n,k}(\tau) \right]. \tag{10}$$

The TD-FDM permits testing of the field $\hat{\mathbf{n}}_m \times \mathbf{H}_{n,k}^s(\mathbf{r}, t)$ generated by the dipole $\mathbf{m}_n(t)$ as

$$\begin{aligned} & \langle \mathbf{m}_m, \hat{\mathbf{n}}_m \times \mathbf{H}_{n,k}^s(\mathbf{r}, t) \rangle \\ &= \frac{1}{4\pi} (\mathbf{m}_m \times \hat{\mathbf{n}}_m) \cdot (\mathbf{m}_n \times \mathbf{R}) \delta(t - R/c) * \left[\frac{\partial_t}{cR^2} + \frac{1}{R^3} \right] I_{n,k}(t), \end{aligned} \tag{11}$$

where $*$ denotes the temporal convolution. Referring to [17], we consider $\delta(t - R/c)$ and expand R using the Taylor series as

$$\delta(t - R/c) = \delta(t - r_m/c) * \delta(t - r_c/c) * \delta(t - r_n/c), \tag{12}$$

where

$$r_m = \left[\hat{\mathbf{r}}_{ji} \cdot \mathbf{r}_{mj} + \frac{(\mathbf{r}_{mj} \cdot \mathbf{r}_{mj}) - (\hat{\mathbf{r}}_{ji} \cdot \mathbf{r}_{mj})^2}{2r_{ji}} \right], \tag{13}$$

$$r_n = \left[-\hat{\mathbf{r}}_{ji} \cdot \mathbf{r}_{ni} + \frac{(\mathbf{r}_{ni} \cdot \mathbf{r}_{ni}) - (\hat{\mathbf{r}}_{ji} \cdot \mathbf{r}_{ni})^2}{2r_{ji}} \right]. \tag{14}$$

Here, $r_c = r_{ji} = |\mathbf{r}_{ji}|$ is the distance between the two group centers and $\hat{\mathbf{r}}_{ji} = \mathbf{r}_{ji}/r_{ji}$. For the amplitude approximation of Eq. (11), $1/R^\alpha$ for $\alpha > 0$ can also be expanded using the Taylor series as

$$\frac{1}{R^\alpha} = \frac{1}{r_{ij}^\alpha} \left[1 - \alpha \left(\frac{\hat{\mathbf{r}}_{ji} \cdot \mathbf{r}_{mj}}{r_{ij}} + \frac{\hat{\mathbf{r}}_{ij} \cdot \mathbf{r}_{ni}}{r_{ij}} \right) \right] = \frac{1}{r_{ij}^\alpha} [x_m^{(\alpha)} + x_n^{(\alpha)}]. \tag{15}$$

With these definitions, substituting Eqs. (7), (12) and (15) into Eq. (11), we can obtain

$$\begin{aligned} & \langle \mathbf{m}_m, \hat{\mathbf{n}}_m \times \mathbf{H}_{n,k}^s(\mathbf{r}, t) \rangle \\ &= \left[x_m^{(3)} (\mathbf{m}'_m \times \mathbf{R}_m) \delta(\tau_m) \right]^\dagger * \left[\frac{\delta(\tau_c)}{4\pi r_c^3} \right] * [\mathbf{m}_n \delta(\tau_n)] * I_{n,k}(t) \end{aligned}$$

$$\begin{aligned}
& + [(\mathbf{m}'_m \times \mathbf{R}_m)\delta(\tau_m)]^\dagger * \left[\frac{\delta(\tau_c)}{4\pi r_c^3} \right] * [x_n^{(3)} \mathbf{m}_n \delta(\tau_n)] * I_{n,k}(t) \\
& + [x_m^{(3)} \mathbf{m}'_m \delta(\tau_m)]^\dagger * \left[\frac{\delta(\tau_c)}{4\pi r_c^3} \right] * [(\mathbf{m}_n \times \mathbf{R}_n)\delta(\tau_n)] * I_{n,k}(t) \\
& + [\mathbf{m}'_m \delta(\tau_m)]^\dagger * \left[\frac{\delta(\tau_c)}{4\pi r_c^3} \right] * [x_n^{(3)} (\mathbf{m}_n \times \mathbf{R}_n)\delta(\tau_n)] * I_{n,k}(t) \\
& + [x_m^{(2)} (\mathbf{m}'_m \times \mathbf{R}_m)\delta(\tau_m)]^\dagger * \left[\frac{\partial_t \delta(\tau_c)}{4\pi c r_c^2} \right] * [\mathbf{m}_n \delta(\tau_n)] * I_{n,k}(t) \\
& + [(\mathbf{m}'_m \times \mathbf{R}_m)\delta(\tau_m)]^\dagger * \left[\frac{\partial_t \delta(\tau_c)}{4\pi c r_c^2} \right] * [x_n^{(2)} \mathbf{m}_n \delta(\tau_n)] * I_{n,k}(t) \\
& + [x_m^{(2)} \mathbf{m}'_m \delta(\tau_m)]^\dagger * \left[\frac{\partial_t \delta(\tau_c)}{4\pi c r_c^2} \right] * [(\mathbf{m}_n \times \mathbf{R}_n)\delta(\tau_n)] * I_{n,k}(t) \\
& + [\mathbf{m}'_m \delta(\tau_m)]^\dagger * \left[\frac{\partial_t \delta(\tau_c)}{4\pi c r_c^2} \right] * [x_n^{(2)} (\mathbf{m}_n \times \mathbf{R}_n)\delta(\tau_n)] * I_{n,k}(t), \quad (16)
\end{aligned}$$

where $\mathbf{m}'_m = \mathbf{m}_m \times \hat{\mathbf{n}}_m$, $\tau_m = t - r_m/c$, $\tau_c = t - r_c/c$, $\tau_n = t - r_n/c$. The superscript \dagger denotes a transpose.

It can be observed that there are eight terms in Eq. (16) and each term has three convolutions. Corresponding to three convolutions, the calculation of each term can be divided into three steps: aggregation; translation; disaggregation. It achieves the separation of the m -th dipole and the n -th dipole. Assuming that there are N_i and N_j unknowns in group G_i and group G_j , the computational complexity of the interactions between G_i and G_j can be reduced from $O(N_i N_j)$ to $O(N_i + N_j)$.

3.2. Implementation of the Multilevel TD-FDM

To implement the multilevel TD-FDM to accelerate the matrix vector products of the RHS in Eq. (5), the algorithm starts by grouping in a multilevel fashion. The whole scatterer must be enclosed in a fictitious cubical box and divided into several equal-sized cubes, which forms the lowest level (level 1). Each cube is then recursively subdivided into eight smaller cubes until the highest level (level l_{\max}). In this way, we finish our multilevel grouping procedure from level 1 to l_{\max} .

For the simplicity of discussion, a two-dimension sketch is used to present the general theory of the multilevel TD-FDM. In Fig. 3, let us take a two level TD-FDM as an example to illustrate how the multilevel TD-FDM works. Each group at level l named parent group is divided into four subgroups named child group and the whole structure is further divided into 36 subgroups.

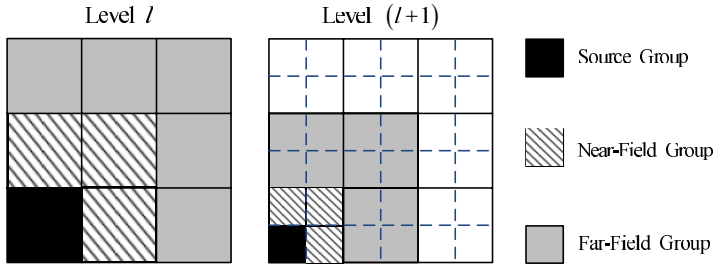


Figure 3. Configuration of the multilevel TD-FDM.

At level $(l+1)$, the computation of interactions between the source group and its near-field groups can be accelerated through the TD-FDM scheme, while this interactions require the direct calculation using the MOT scheme at level l . Then the near-field group pairs at level $(l+1)$ can be again divided into four smaller subgroups, which generates the new far-field group pairs. Until the highest level, all the near-region interactions should be calculated directly using the MOT scheme.

From the above discussion, at each level all group pairs $(\alpha(l), \alpha'(l))$ ($\alpha(l) \in R(l)$) require to perform the aggregation-translation-disaggregation procedure. Here $R(l)$ is a set of groups at level l , in which $\alpha(l)$ satisfies the condition that $\alpha(l)$ and $\alpha'(l)$ are far-field pair and their parent group $\alpha(l-1)$ and $\alpha'(l-1)$ do not qualify as far-field pair. Then the multilevel TD-FDM can be expressed as the sums of near-field evaluation and far-field evaluation

$$\sum_{j=0}^{i-1} \mathbf{z}_{i-j} \mathbf{I}_j = \sum_{j=0}^{i-1} \mathbf{z}_{i-j}^{\alpha(l_{\max}), \alpha'(l_{\max})} I_j^{\alpha'(l_{\max})} + \sum_{l=1}^{l_{\max}} \sum_{p=1}^8 \sum_{\alpha(l) \in R(l)} \mathbf{M}_m^{p,(l)} \delta(\tau_m) * \mathbf{T}^{p,(l)} \delta(\tau_c) * \sum_{\alpha'(l)} \mathbf{M}_n^{p,(l)} \delta(\tau_n) * I_{n,k}(t)|_{t=i\Delta t}, \quad (17)$$

where $\mathbf{M}_m^{p,(l)}$, $\mathbf{T}^{p,(l)}$ and $\mathbf{M}_n^{p,(l)}$ for $1 \leq p \leq 8$ denote eight aggregation-translation-disaggregation operation in Eq. (16).

In our practical implementation, the appropriate subsignal duration must be defined first. Because the distance between the closest far-field pair vary at different levels, the fundamental subsignal duration are also different at each level. The level l subsignal duration $T_s^{(l)}$ can be defined as

$$T_s^{(l)} = M_t^{(l)} \Delta t = \left(\left\lfloor \frac{\beta D(l)}{c \Delta t} \right\rfloor - 1 \right) \Delta t. \quad (18)$$

Here, $D(l)$ is the size of the level l group, and β is the threshold. The larger β is, the more costly and accurate the algorithm becomes.

After $T_s^{(l)}$ has been defined, the level l far-field evaluation of Eq. (17) is divided into 3 steps: aggregation, translation and disaggregation.

(1) Aggregation: For each pair $(\alpha(l), \alpha'(l))$ ($\alpha(l) \in R(l)$), level l outgoing rays $V_1^{(l)}(t)$ generated by subsignals of the duration $T_s^{(l)}(l)$ are constructed every $M_t^{(l)}$ time steps. This contribution aggregating the signal from the n -th equivalent dipole to the level l group center $O_i^{(l)}$ can be obtained by the rightmost convolution of Eq. (17)

$$V_1^{(l)}(t) = \left[\mathbf{M}_n^{p,(l)} \delta(t - r_n/c) \right] * I_{n,k}(t). \quad (19)$$

(2) Translation: Once outgoing rays $V_1^{(l)}(t)$ aggregated for each far-field pair, outgoing rays are immediately translated from the level l group center $O_i^{(l)}$ to the level l group center $O_j^{(l)}$. Each outgoing ray is converted to an incoming ray by the middle convolution of Eq. (17)

$$V_2^{(l)}(t) = \left[\mathbf{T}^{p,(l)} \delta(t - r_c/c) \right] * V_1^{(l)}(t), \quad (20)$$

where $\mathbf{T}^{p,(l)} \delta(t - r_c/c)$ is termed the translation operator, and $V_2^{(l)}(t)$ represents level l incoming rays.

(3) Disaggregation: Finally at each time step, the field at the observer can be formed by the left convolution of Eq. (17)

$$V_3^{(l)}(t) = \left[\mathbf{M}_m^{p,(l)} \delta(t - r_m/c) \right] * V_2^{(l)}(t). \quad (21)$$

This process disaggregates the incoming rays from the level l group center $O_j^{(l)}$ to the m -th equivalent dipole. This process involves a very similar operation to the aggregation process.

Like the single level TD-FDM, there are three temporal convolutions. Each convolution operation is nothing but a time shift. These convolutions do not require using fast Fourier transforms and it can be carried out in the time domain.

4. NUMERICAL RESULTS

This section provides several numerical results that serve both to validate the multilevel TD-FDM and to demonstrate its efficiency. All simulations are performed on a shared memory workstation equipped with Intel(R) Xeon(R) Dual CPU W5580 3.2 GHz (only one core is used) and 28 GB of RAM. In our implementation, we use the generalized minimal residual (GMRES) iterative solver for each time step and choose the identical residual error $\leq 10^{-6}$. The temporal basic function $T(t)$ is constructed using third order Lagrange

interpolation [20]. All examples herein are calculated by the 2-level TD-FDM and the threshold is chosen $\beta = 3$. With the number of level increasing, the group size and the error of the Taylor series approximation will also increase, so it requires the larger β [18].

In the first example, we consider a square plate with dimension $6.0\text{ m} \times 6.0\text{ m} \times 0.1\text{ m}$. The surface of the scatterer is discretized in terms of 31458 RWG basis functions. The incident wave is a Gaussian plane wave parameterized as $\mathbf{E}^i(\mathbf{r}, t) = \hat{\mathbf{p}} \frac{4}{T_0\sqrt{\pi}} \exp[-\frac{16}{T_0^2}(ct - ct_0 - \mathbf{r} \cdot \hat{\mathbf{k}})^2]$. Here $T_0 = 4\text{ ns}$ is the pulsewidth of the Gaussian impulse, $ct_0 = 6\text{ m}$ is the time delay, $\hat{\mathbf{k}} = -\hat{\mathbf{z}}$ denotes the travel direction of the incident wave, and $\hat{\mathbf{p}} = -\hat{\mathbf{x}}$ is a unit vector of its polarization. The size of level l_{\max} group is 0.3 m , the time step size is 166.6 ps , and $N_t = 4000$. Both CPU time and memory requirement of each method are listed in Table 1. The current density for x direction observed at the point $(0\text{ m}, 0\text{ m}, 0\text{ m})$ computed using both the TD-FDM and the multilevel TD-FDM are compared in Fig. 4. The back-scattered far field signal for x direction are compared in Fig. 5. The results are in good agreement with each other.

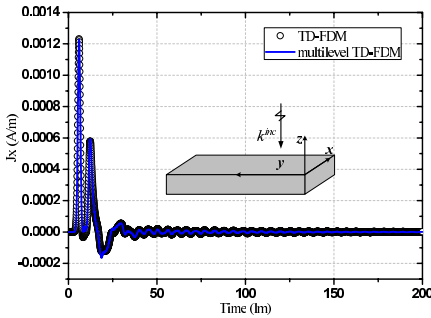


Figure 4. The current density at $(0\text{ m}, 0\text{ m}, 0\text{ m})$.

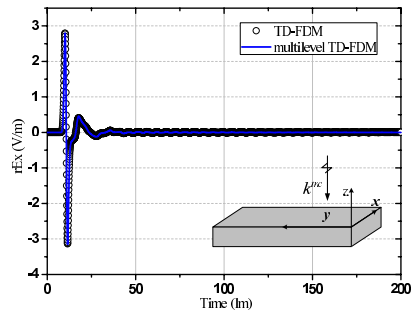


Figure 5. Back-scattered far field response.

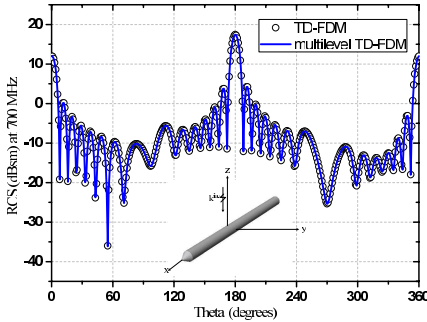
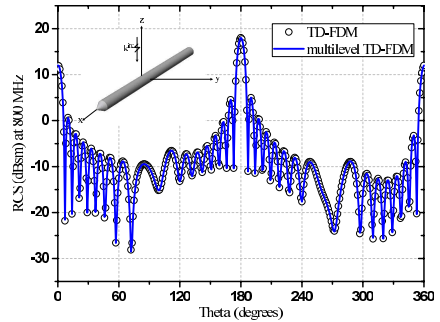
Next, to further verify the validity of the multilevel TD-FDM, scattering from a PEC pencil target is analyzed. The pencil consisted of a 3 m long cylinder with radius 0.1 m , and a tip extending 0.173 m pointing toward $+x$ direction. The object is discretized into 31947 RWG basis functions. The incident wave is a modulated Gaussian plane wave parameterized as $\mathbf{E}^i(\mathbf{r}, t) = \hat{\mathbf{p}} \exp[-\frac{1}{2\sigma^2}(\tau_0 - 8\sigma)^2] \cos(2\pi f_0\tau_0)$. Here $f_0 = 800\text{ MHz}$ is the center frequency, $f_{bw} = 300\text{ MHz}$ is the bandwidth of the signal, $\sigma = 6/(2\pi f_{bw})$, and $\tau_0 = t - \mathbf{r} \cdot \hat{\mathbf{k}}/c$. The size of level l_{\max} group is 0.09 m , the time step size is 50 ps , and $N_t = 8000$. The RCS was computed for $\phi = 0^\circ$, and θ between 0° and 360° . The bistatic RCS patterns at 700 MHz ,

Table 1. Comparison of CPU time and memory cost.

Example 1		
Method	CPU Time	RAM
TD-FDM	7 h 48 m	19.1 GB
Multilevel TD-FDM	4 h 26 m	9.8 GB
Example 2		
Method	CPU Time	RAM
TD-FDM	14 h 32 m	19.2 GB
Multilevel TD-FDM	9 h 37 m	13.7 GB
Example 3		
Method	CPU Time	RAM
TD-FDM	—	—
Multilevel TD-FDM	8 h 02 m	18.9 GB

800 MHz, and 900 MHz obtained by the multilevel TD-FDM agree well with TD-FDM as shown in Figs. 6–8.

The last example considers a 22-by-22 array of conducting cube with side length of 0.3 m. The array is discretized into 78408 RWG basis functions. The incident wave is a modulated Gaussian pulse with $\hat{\mathbf{p}} = -\hat{\mathbf{x}}$, $\hat{\mathbf{k}} = -\hat{\mathbf{z}}$, $f_0 = 250$ MHz, $f_{bw} = 100$ MHz, and $\sigma = 6/(2\pi f_{bw})$. Due to the limit of memory, the target cannot be calculated by the TD-FDM. The size of level l_{\max} group is 0.3 m, $\Delta t = 666.6$ ps, and $N_t = 1000$. The CPU time and memory requirement are listed in Table 1. The current density for x direction observed at the points (1.5 m, 1.8 m, 0.0 m) and (4.5 m, 0.0 m, 0.0 m) are shown in Figs. 9 and 10.

**Figure 6.** Comparison of the bistatic RCS at 700 MHz.**Figure 7.** Comparison of the bistatic RCS at 800 MHz.

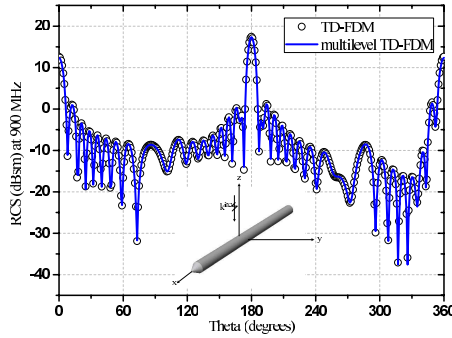


Figure 8. Comparison of the bistatic RCS at 900 MHz.

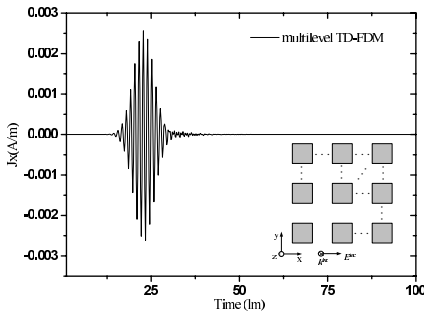


Figure 9. The current density at (1.5 m, 1.8 m, 0.0 m).

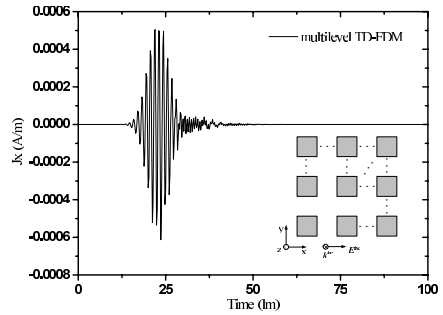


Figure 10. The current density at (4.5 m, 0.0 m, 0.0 m).

5. CONCLUSIONS

In this paper, the multilevel TD-FDM is proposed to solve the MFIE for the electromagnetic scattering from the PEC targets. All the far-region computation at each level are speeded up by the TD-FDM, and the near-region interaction at the highest level are computed by the MOT scheme. Compared with the single level TD-FDM, both the memory requirement and CPU time are reduced. Numerical results demonstrate the validity and efficiency of our method. Further more, the multilevel TD-FDM can be easily extended to solve volume integral equation for isotropic media.

ACKNOWLEDGMENT

This work is supported by the National Natural Science Foundation of China under Grant No. 61071019, the National Natural Science Foundation of China for Young Scholars under Grant No. 61102033, the

Fundamental Research Funds for the Central Universities under Grant NS2012096 and the Foundation of State Key Laboratory of Millimeter Waves, Southeast University, P. R. China under Grant No. K201302.

REFERENCES

1. Rao, S. M. and D. R. Wilton, "Transient scattering by conducting surfaces of arbitrary shape," *IEEE Trans. on Antennas and Propagat.*, Vol. 39, No. 1, 56–61, Jan. 1991.
2. Shanker, B., A. A. Ergin, K. Aygun, and E. Michielssen, "Analysis of transient electromagnetic scattering from closed surfaces using a combined field integral equation," *IEEE Trans. on Antennas and Propagat.*, Vol. 48, No. 7, 1064–1074, Jul. 2000.
3. Jung, B. H., Z. Mei, and T. K. Sarkar, "Transient wave propagation in a general dispersive media using the laguerre function in a marching-on-in-degree (MOD) methodology," *Progress In Electromagnetics Research*, Vol. 118, 135–149, 2011.
4. Luo, W., W. Y. Yin, M. D. Zhu, and J. Y. Zhao, "Hybrid TDIE-TDPO method for studying on transient responses of some wire and surface structures illuminated by an electromagnetic pulse," *Progress In Electromagnetics Research*, Vol. 116, 203–219, 2011.
5. Zhu, H., Z. H. Wu, X. Y. Zhang, and B. J. Hu, "Time-domain integral equation solver for radiation from dipole antenna loaded with general bi-isotropic objects," *Progress In Electromagnetics Research B*, Vol. 35, 349–367, 2011.
6. Zhu, M. D., X. L. Zhou, W. Luo, and W. Y. Yin, "Hybrid TDIE-TDPO method using weighted Laguerre polynomials for solving transient electromagnetic problems," *Progress In Electromagnetics Research*, Vol. 126, 375–398, 2012.
7. Sirenko, K., V. Pazynin, Y. Sirenko, and H. Bagci, "An FFT-accelerated FDTD scheme with exact absorbing conditions for characterizing axially symmetric resonant structures," *Progress In Electromagnetics Research*, Vol. 111, 331–364, 2011.
8. Wang, J. B., B. H. Zhou, L. H. Shi, C. Gao, and B. Chen, "A novel 3-D weakly conditionally stable FDTD algorithm," *Progress In Electromagnetics Research*, Vol. 130, 525–540, 2012.
9. Ergin, A. A., B. Shanker, and E. Michielssen, "The plane wave time-domain algorithm for the fast analysis of transient wave phenomena," *IEEE Antennas Propagat. Mag.*, Vol. 41, No. 4, 39–52, Sept. 1999.
10. Shanker, B., A. A. Ergin, K. Aygun, and E. Michielssen, "Analysis of transient electromagnetic scattering phenomena using a two-

- level plane wave time domain algorithm,” *IEEE Trans. on Antennas and Propagat.*, Vol. 48, No. 4, 510–523, Apr. 2000.
11. Shanker, B., A. A. Ergin, M. Y. Lu, and E. Michielssen, “Fast analysis of transient electromagnetic scattering phenomena using the multilevel plane wave time domain algorithm,” *IEEE Trans. on Antennas and Propagat.*, Vol. 51, No. 3, 628–641, Mar. 2003.
 12. Yilmaz, A. E., J. M. Jin, and E. Michielssen, “Time domain adaptive integral method for surface integral equations,” *IEEE Trans. on Antennas and Propagat.*, Vol. 52, No. 10, 2692–2708, Oct. 2004.
 13. Yilmaz, A. E., J. M. Jin, and E. Michielssen, “Analysis of low-frequency electromagnetic transients by an extended time-domain adaptive integral method,” *IEEE Trans. on Advanced Packaging*, Vol. 30, No. 2, 301–312, May 2007.
 14. Ding, J., C. Gu, Z. Niu, and Z. Li, “Application of the equivalent dipole moment method for transient electromagnetic scattering,” *International Conference on Microwave and Millimeter Wave Technology, ICMMT 2012*, Vol. 3, 898–900, 2012.
 15. Ding, J., C. Gu, Z. Li, and Z. Niu, “Analysis of transient electromagnetic scattering using time domain equivalent dipole moment method,” *Journal of Electromagnetic Waves and Applications*, Vol. 27, No. 1, 39–47, 2013.
 16. Ding, J., C. Gu, Z. Li, and Z. Niu, “Analysis of transient electromagnetic scattering using time domain fast dipole method,” *Progress In Electromagnetics Research*, Vol. 136, 543–559, 2013.
 17. Chen, X., C. Gu, Z. Niu, and Z. Li, “Fast dipole method for electromagnetic scattering from perfect electric conducting targets,” *IEEE Trans. on Antennas and Propagat.*, Vol. 60, No. 2, 1186–1191, Feb. 2012.
 18. Chen, X., Z. Li, Z. Niu, and C. Gu, “Multilevel fast dipole method for electromagnetic scattering from perfect electric conducting targets,” *IET Microw. Antennas Propagat.*, Vol. 6, No. 3, 263–268, 2012.
 19. Chen, X., Z. Li, Z. Niu, and C. Gu, “Analysis of electromagnetic scattering from PEC targets using improved fast dipole method,” *Journal of Electromagnetic Waves and Applications*, Vol. 25, No. 16, 2254–2263, 2012.
 20. Aygun, K., M. Lu, B. Shanker, and E. Michielssen, “Analysis of PCB level EMI phenomena using an adaptive low-frequency plane wave time domain algorithm,” *IEEE International Symposium on Electromagnetic Compatibility*, Vol. 1, 295–300, 2000.